Bioorganic Chemistry 138 (2023) 106607

Contents lists available at ScienceDirect

Bioorganic Chemistry

journal homepage: www.elsevier.com/locate/bioorg

Targeting the Grb2 cSH3 domain: Design, synthesis and biological evaluation of the first series of modulators

Marianna Bufano [a], Michela Puxeddu [a], Marianna Nalli [a], Giuseppe La Regina [a], Angelo Toto [b], Francesca Romana Liberati [b], Alessio Paone [b], Francesca Cutruzzolà [b], Domiziana Masci [c], Chiara Bigogno [d], Giulio Dondio [d], Romano Silvestri [a], Stefano Gianni [b], Antonio Coluccia [a,*]

[a] Dipartimento di Chimica e Tecnologie del Farmaco, Sapienza Università di Roma, Laboratory affiliated to Istituto Pasteur Italia – Fondazione Cenci Bolognetti, Piazzale Aldo Moro 5, I-00185 Roma, Italy

[b] Dipartimento di Scienze Biochimiche "A. Rossi Fanelli" and Istituto di Biologia e Patologia Molecolari del CNR, Sapienza Università di Roma, Laboratory affiliated to Istituto Pasteur Italia – Fondazione Cenci Bolognetti Piazzale Aldo Moro 5, I-00185 Roma, Italy

[c] Department of Basic Biotechnological Sciences, Intensivological and Perioperative Clinics, Catholic University of Sacred Heart, Largo Francesco Vito 1, 00168 Rome, Italy

[d] Aphad SrL, Via della Resistenza 65, 20090 Buccinasco, Italy

ARTICLE INFO

Keywords:
Grb2-Gab2 system
SH3 domain
Anticancer
Small Molecules
Structure activity Relationship

ABSTRACT

Growth factor receptor bound protein 2 (Grb2) is an adaptor protein featured by a nSH3-SH2-cSH3 domains. Grb2 finely regulates important cellular pathways such as growth, proliferation and metabolism and a minor lapse of this tight control may totally change the entire pathway to the oncogenic. Indeed, Grb2 is found overexpressed in many tumours type. Consequently, Grb2 is an attractive therapeutic target for the development of new anticancer drug.

Herein, we reported the synthesis and the biological evaluation of a series of Grb2 inhibitors, developed starting from a hit-compound already reported by this research unit. The newly synthesized compounds were evaluated by kinetic binding experiments, and the most promising derivatives were assayed in a short panel of cancer cells. Five of the newly synthesized derivatives proved to be able to bind the targeted protein with valuable inhibitory concentration in one-digit micromolar concentration. The most active compound of this series, derivative **12**, showed an inhibitory concentration of about 6 μM for glioblastoma and ovarian cancer cells, and an IC_{50} of 1.67 for lung cancer cell. For derivative **12**, the metabolic stability and the ROS production was also evaluated. The biological data together with the docking studies led to rationalize an early structure activity relationship.

1. Introduction

Growth factor receptor bound protein 2 (Grb2) is a 25 kDa adaptor protein, which transports the membrane stimuli from cytoplasm to the nucleus acting as bridge between receptor tyrosine kinases (RTK) and gene transcription pathways. [1] This crucial cellular activity relies on a peculiar structure: Grb2 has one Src homology 2 (SH2) domain flanked by two Src homology 3 (SH3) domains. [2,3] The SH2 domain specifically binds to phosphorylated tyrosine (pY) residue of several receptor tyrosine kinases, which include, among others, the epidermal growth factor receptor (EGFR) and the platelet-derived growth factor receptor (PDGFR). [4] In the unbound state, Grb2 has an autoinhibited conformation that turns to active after pY-containing motif bind to SH2. In the active conformation the nSH3/cSH3 domains became available for interactions with downstream effectors. [4,5] The nSH3 domain binds Son of Sevenless1 (SOS1) protein, which in turns activates the Ras/MAPK and PI3K/AKT signal cascade. This pathway has a crucial role in the tuning of cellular growth and differentiation. [6] The cSH3 domain binds and activates the Grb2-associated binding protein (Gab2). [7] The activated form of Gab2 turns on RAS, PI3K and JAK pathways. It is well documented that these pathways have a crucial role in many cellular processes and are involved in cancer genesis. [8-10] Indeed, Gab2 is overexpressed in many cancer types such as breast [11] gastric [12] and lung [13] and haematological cancers. [14-16] It was also

* Corresponding author.
E-mail address: antonio.coluccia@uniroma1.it (A. Coluccia).

https://doi.org/10.1016/j.bioorg.2023.106607
Received 23 March 2023; Received in revised form 5 May 2023; Accepted 8 May 2023
Available online 11 May 2023

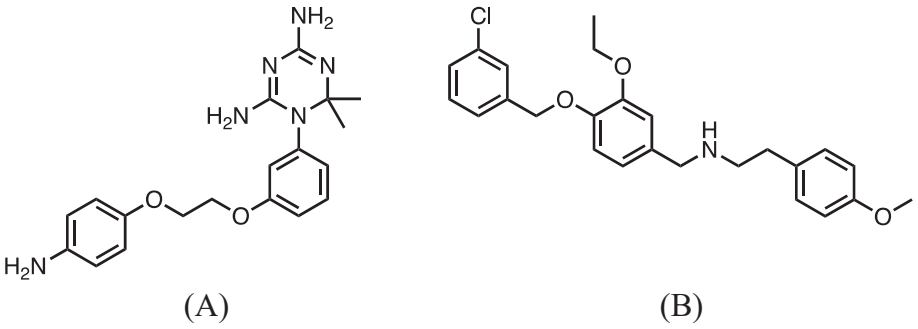

Fig. 1. Structure of cSH3 modulators. (A) diphenyl triazine derivative (B) AN-465-J137-985 (**1**).

Table 1
Structure of the reported compounds.

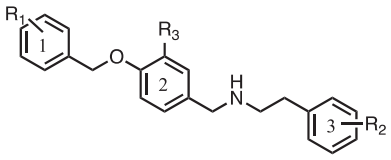

Compound	R_1	R_2	R_3
1	3-Cl	4-OCH_3	OEt
2	H	H	OEt
3	3-Cl	3-OCH_3	OEt
4	3-Cl	2-OCH_3	OEt
5	3-Cl	H	OEt
6	4-Cl	4-OCH_3	OEt
7	2-Cl	4-OCH_3	OEt
8	H	4-OCH_3	OEt
9	3-Cl	2-Cl	OEt
10	3-Cl	3-Cl	OEt
11	3-Cl	4-Cl	OEt
12	3-CH_3	4-OCH_3	OEt
13	4-CH_3	4-OCH_3	OEt
14	2-CH_3	4-OCH_3	OEt
15	2-OCH_3	4-OCH_3	OEt
16	3-OCH_3	4-OCH_3	OEt
17	4-OCH_3	4-OCH_3	OEt
18	3-Cl	4-OCH_3	H
19	3-OCH_3	4-Cl	OEt

reported that the knock down of Gab2 in animal model of ovarian and lung cancer inhibited tumour cell proliferation, angiogenesis and metastatic potential. [17,18].

Considering the involvement of Grb2 in progression and development of multiple malignancies [19-22] and the role of its effectors Gab2 [11-17] the Grb2/Gab2 complex became a very attractive therapeutic target. [17].

In literature are reported many examples of nSH3 binders to modulate the Grb2/SOS1 complex [1]. It is also widely explored the research of SH2 inhibitors able to impair the interaction between Grb2 and pY-containing proteins. [23-27] On the contrary, just two cSH3 modulators are reported to date: a diphenyl triazine derivative with an IC_{50} 320 μM, which was not further developed (Fig. 1A) [28] and derivative AN-465-J137-985 (**1**) recently identified by this research group. [29] (Fig. 1B) Compound **1** proved to bind the cSH3 domain, to impar the Grb2/Gab2 interaction and to inhibit the proliferation of the tested lung cancer cell lines (H1299 and A549) at one-digit micromolar concentration (5 and 7 μM respectively). [29].

Starting from the promising results of derivative **1**, a new series of analogues was designed and synthesized. Molecular modelling studies were accomplished to clarify the structural activity relationship risen from the biological assays. Five out of the 18 tested compounds showed valuable inhibitory activity in the range of one-digit micromolar concentration. The most active compound of this new series, derivative **12** had an IC_{50} of 1.60 μM for H1299 lung cancer cell line.

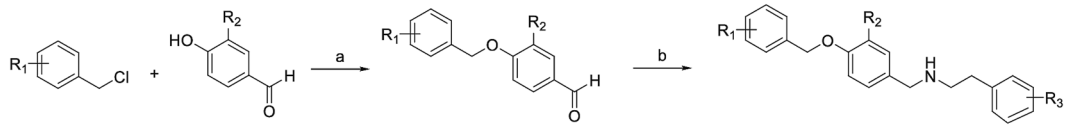

R_1 = Cl, Me, OMe **R_2** = OMe, H

20: R_1 = H; R_2 = OEt
21: R_1 = *m*-Cl; R_2 = OEt
22: R_1 = *p*-Cl; R_2 = OEt
23: R_1 = *o*-Cl; R_2 = H
24: R_1 = *m*-Me; R_2 = OEt
25: R_1 = *p*-Me; R_2 = OEt
26: R_1 = *o*-Me; R_2 = OEt
27: R_1 = *o*-OMe; R_2 = OEt
28: R_1 = *m*-OMe; R_2 = OEt
29: R_1 = *p*-OMe; R_2 = OEt
30: R_1 = *m*-Cl; R_2 = H

2: R_1 = H; R_2 = OEt; R_3 = H
3: R_1 = *m*-Cl; R_2 = OEt; R_3 = *m*-OMe
4: R_1 = *m*-Cl; R_2 = OEt; R_3 = *o*-OMe
5: R_1 = *m*-Cl; R_2 = OEt; R_3 = H
6: R_1 = *p*-Cl; R_2 = OEt; R_3 = *p*-OMe
7: R_1 = *o*-Cl; R_2 = OEt; R_3 = *p*-OMe
8: R_1 = H; R_2 = OEt; R_3 = *p*-OMe
9: R_1 = *m*-Cl; R_2 = OEt; R_3 = *p*-OMe
10: R_1 = *m*-Cl; R_2 = OEt; R_3 = *m*-Cl
11: R_1 = *m*-Cl; R_2 = OEt; R_3 = *p*-Cl
12: R_1 = *m*-Me; R_2 = OEt; R_3 = *p*-OMe
13: R_1 = *p*-Me; R_2 = OEt; R_3 = *p*-OMe
14: R_1 = *o*-Me; R_2 = OEt; R_3 = *p*-OMe
15: R_1 = *o*-OMe; R_2 = OEt; R_3 = *p*-OMe
16: R_1 = *m*-OMe; R_2 = OEt; R_3 = *p*-OMe
17: R_1 = *p*-OMe; R_2 = OEt; R_3 = *p*-OMe
18: R_1 = *m*-Cl; R_2 = H; R_3 = *p*-OMe
19: R_1 = *m*-OMe; R_2 = OEt; R_3 = *p*-Cl

Scheme 1. General synthesis of compounds **2-19**[a] [a)] Reagents and condictiones: a) **20–30**: Cs_2CO_3, *N*,*N*-dimethylformamide, 70 °C, 1 h, 76–99%; b) **2–19**: *i* appropriate phenethyl ammine, 3 Å molecular sieves, ethanol absolute, 1.5 h, 25 °C, *ii* $NaBH_4$ 25 °C, 1 h, 22–70%.

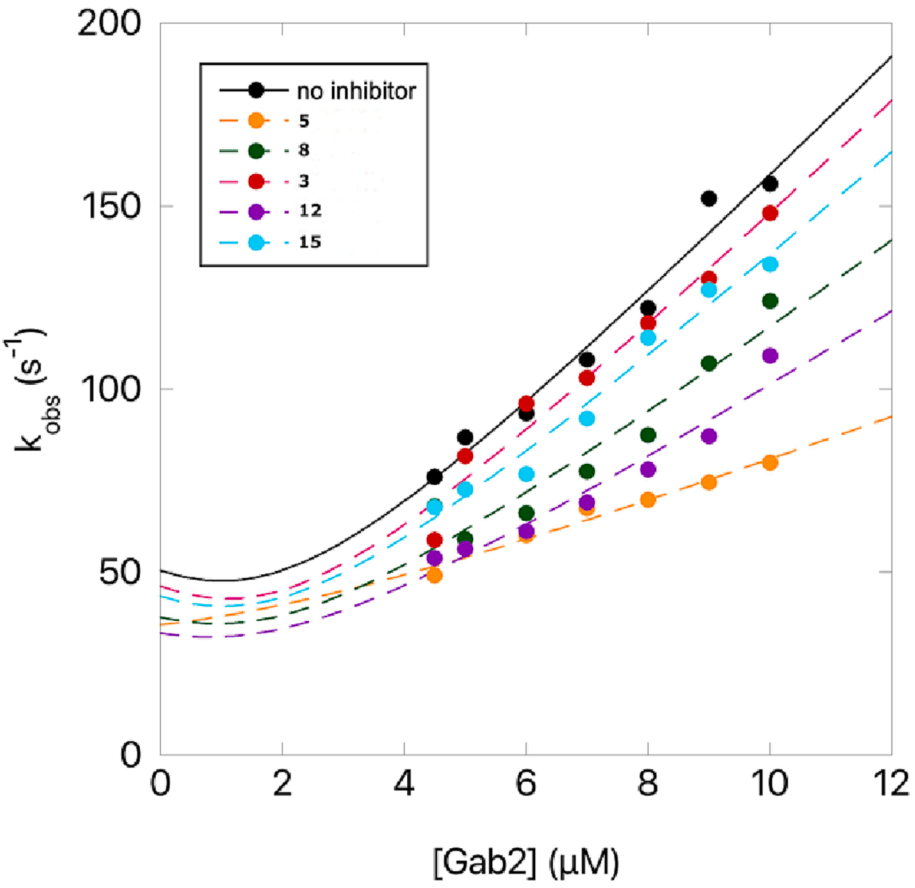

Fig. 2. Observed rate constants measured through stopped-flow kinetic binding experiments by rapidly mixing a constant concentration of cSH3 versus different concentrations of Gab2* in absence and in presence of fixed concentration (5 μM) of each inhibitor. Lines are the best fit to Equation 1.

2. Results

Recently, derivative **1** (Table 1) was identified by this research unit through a virtual screening procedure. [29] The binding mode of compound **1** was deeply investigated by docking and molecular dynamic. The results of simulations suggested that both the secondary nitrogen amine and the three phenyl rings had a crucial role in the binding. (Fig. 1SI) [29] The computations did not give confident information about the role of the substituents at the phenyl rings. The only consistent data was that small substituents were well accepted, whereas the introduction of bulky groups markedly affected the binding mode. Thus, with the aim to better understand the effect of the substituents, small moieties like -Cl, $–CH_3$ and OCH_3 were used to modify the phenyl rings of derivative **1**. (Table 1).

2.1. Synthesis

Compounds **2**–**19** were prepared by reacting intermediate **20**–**30** with the appropriate phenethyl amine in ethanol for 1.5 h. Then $NaBH_4$ was added and the mixture was stirred for 1 h at rt. Intermediate **20**–**30** were synthesized by reacting ethyl vanilline, or 4-hydroxybenzaldehyde (**30**) with appropriate benzyl chloride in the presence of caesium carbonate in *N,N*-dimethylformammide at 70 °C for 1 h. (Scheme 1).

2.2. Biological evaluation

All the newly synthesized derivatives were employed in equilibrium binding experiments to test their ability to modulate the binding reaction between cSH3 domain of Grb2 and Gab2. In these experiments, a constant concentration of cSH3 (1 μM) was mixed with increasing concentrations of dansylated $Gab2_{503\text{-}524}$ (from 1 μM to 20 μM), in the absence and presence of a constant concentration (5 μM) of inhibitor molecules (**2**–**19**). Samples were excited at 280 nm and the quenching of Trp fluorescence emission by the dansylated peptide was followed. Data obtained at 340 nm wavelength was plotted as function of dansylated peptide concentration and satisfactorily fitted with a hyperbolic function, (Fig. 2SI). Of all the molecules tested, only molecules **3**, **5**, **8**, **12**, and **15** showed an appreciable effect on the affinity of cSH3 for $Gab2_{503\text{-}524}$ (Fig. 2 SI), so that they were used in stopped-flow kinetic binding

Table 2
Kinetic and cellular data of the most potent inhibitors.

Compound	k_{on}^{a} (μM^{-1} s^{-1})	k_{off} (s^{-1})	K_D (μM)	IC_{50} (μM)[c]		
				H1299	SKOV3	U87
No inhibitor	16.8 ± 1.0	6.1 ± 0.1	0.35 ± 0.04			
1	–	–	–	3.64	5.87	7.51
3	16.0 ± 1.0	7.5 ± 0.2	0.2 ± 0.1	6.27	6.31	10
5	6.3 ± 0.5	6.3 ± 0.1	1.2 ± 0.1	9.82	7.41	7.17
8	12.0 ± 1.0	6.6 ± 0.2	0.21 ± 0.05	12.05	8.81	7.24
12	10.5 ± 0.9	6.8 ± 0.2	0.27 ± 0.04	1.67	6.12	6.15
15	14.6 ± 0.8	7.0 ± 0.1	0.18 ± 0.06	8.21	7.57	6.98

[a]Stopped-flow kinetic binding experiments; [b]equilibrium binding experiments; [c]each experiment have been repeated in triplicate.

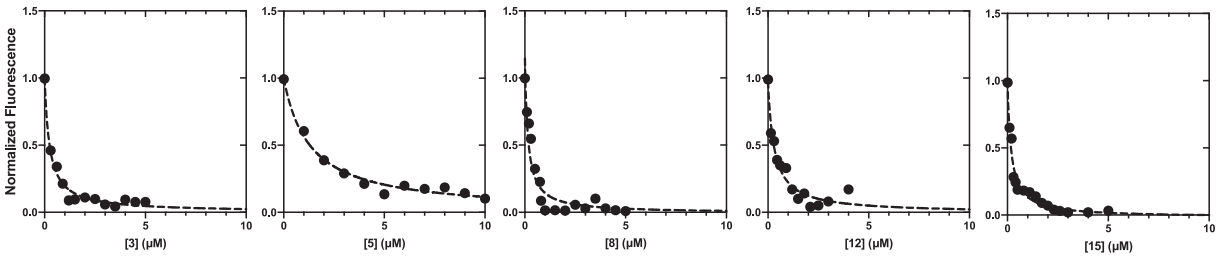

Fig. 3. Equilibrium binding experiments conducted by mixing a constant concentration of cSH3 versus increasing concentrations of inhibitor molecules. Broken lines are the best fit to a hyperbolic function.

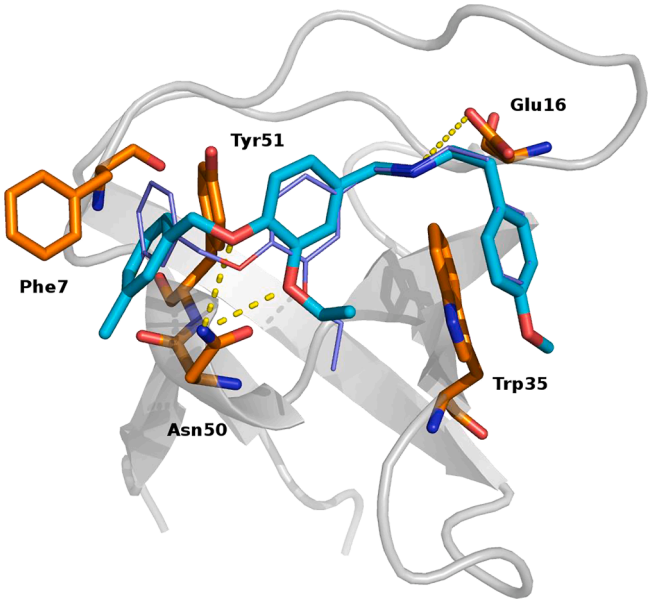

Fig. 4. Proposed binding mode for derivative **1** and **12.** Derivative **1** is reported in purple lines. Derivatives **12** (cyan) is reported in stick. C-SH3 domain of Grb2 protein is reported as grey cartoon. Residues involved in interactions are reported as orange stick. The polar interactions H-bond and salt bridge are reported as yellow dot lines. (For interpretation of the references to colour in this figure legend, the reader is referred to the web version of this article.)

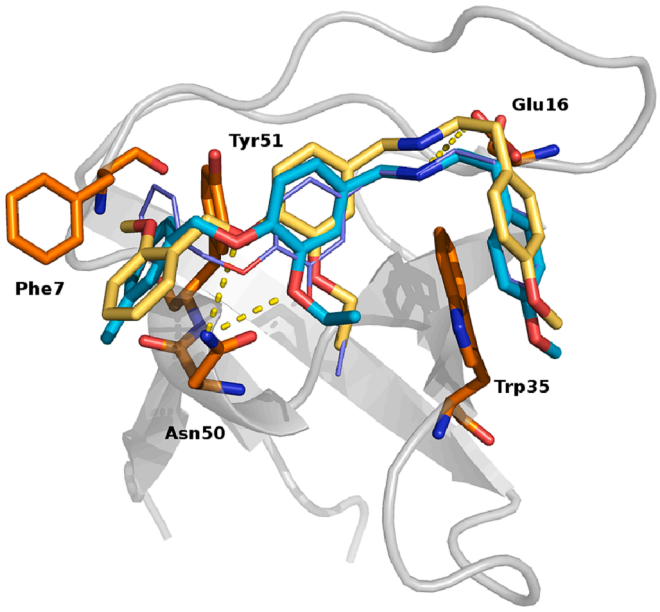

Fig. 5. Proposed binding mode for derivative **12** (cyan), and **15** (yellow). Derivative **1** is reported in purple lines. Residues involved in interactions are reported as orange stick. C-SH3 domain of Grb2 protein is depicted as grey cartoon. The polar interactions H-bond and salt bridge are reported as yellow dot lines. (For interpretation of the references to colour in this figure legend, the reader is referred to the web version of this article.)

experiments, to monitor their possible effect on the early events of the recognition or late complex stabilization of the binding reaction. A constant concentration of cSH3 (1 μM) was rapidly mixed with increasing concentrations of dansylated $Gab2_{503\text{-}524}$ (from 4 μM to 10 μM), in the absence and presence of a constant concentration (5 μM) of inhibitor molecules (Fig. 2). The obtained observed rate constants (k_{obs}) were then plotted as a function of peptide concentration and fitted using the following equation. (Eq. 1).

Eq. 1. [30]

$$k_{obs} = sqrt(k_{on}^2(2 - [peptide]\,)^2 + k_{off}^2 + 2k_{on}k_{off}(2 + [peptide]\,))$$

Thus, we calculated the microscopic association rate constant (k_{on}) and the microscopic dissociation rate constant (k_{off}). In order to directly calculate the k_{off} we performed displacement experiments [31] by rapidly mixing a preincubated complex of cSH3 and dansylated $Gab2_{503\text{-}524}$ with an excess of non-dansylated $Gab2_{503\text{-}524}$, in the absence or presence of a constant concentration (5 μM) of inhibitor molecule. The calculated k_{on} and k_{off} values are reported in Table 2.

As a further step, we conducted equilibrium binding experiments to test the ability of the cSH3 domain to directly interact with the tested molecules. Experiments were conducted by challenging a fixed concentration of cSH3 domain (1 μM) versus increasing concentrations of inhibitors, exciting the sample at 280 nm and following the change in intrinsic fluorescence of cSH3 at 342 nm. Obtained data are reported in Fig. 3 and confirm the ability of the cSH3 domain to bind molecules **3** ($K_D = 0.2 \pm 0.1$ μM),**5** ($K_D = 1.2 \pm 0.1$ μM), **8** ($K_D = 0.21 \pm 0.05$ μM), **12** ($K_D = 0.27 \pm 0.04$) and **15** ($K_D = 0.18 \pm 0.06$ μM).

The same compounds were then evaluated in three different cancer cell lines: H1299 (lung carcinoma), SKOV3 (ovarian cancer), and U87 (glioblastoma) to measure the antiproliferative activity. (Table 2).

The results obtained on the cells were in good accordance with the binding assays. All the selected compounds showed a relevant inhibitory concentration for all the studied cell lines. (Figs. 3-5 SI) The measured IC_{50} fall in the range of one-digit micromolar concentration, with the only exception of derivative **8** that had a IC_{50} of 12.05 μM for the H1299 cell line. Compound **12** showed the lower inhibitory concentrations for H1299, SKOV3 and U87 cells with a IC_{50} of 1.67, 6.12, and 6.15 μM respectively. In general, the compounds showed biological activity values close to these of the reference compound **1**.

2.3. Structure activity relationship

The analysis biological activity data and the docking studies drove the outline of a structure activity relationship.

Firstly, the substitution of the ethoxy moiety at the central phenyl ring (ring 2) gave rise to inactive compound (compare **18** with **1**).

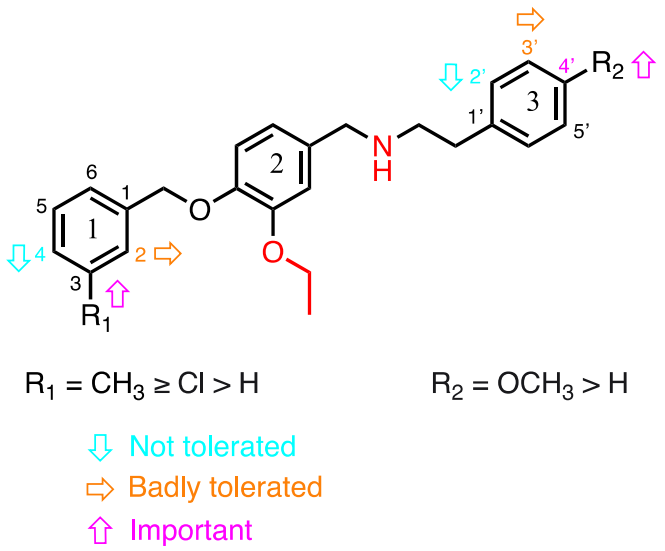

Fig. 6. Summary of Structure Activity Relationship.

Indeed, the derivative **18** was not able to affect the binding of $Gab2_{503-524}$ (Table 1 SI). Worthily, the docking computation suggested for **18** an unrelated binding mode compared with the one described for reference compound (data not shown). In the same way, the simultaneous replacement of the 3-chlorine atom of ring 1 and the 4′-methoxy group of ring 3 completely abolished the biological activity (compare **2** with **1** and **12**). Also, the substitution of one at time of these two groups (**5** and **8**) produced a slight increment of the inhibitory concentration values, despite this did not affect the binding mode (Table 3). These data confirmed the crucial role of a proper substitution at the phenyl rings.

Then, it was explored the effect of chlorine, methyl and methoxy groups in the different positions of ring 1 keeping the 4′-methoxy moiety at ring 3. The introduction of a substituent in position 4 of phenyl ring 1 was always detrimental to the biological activity, providing inactive compounds (**6**, **13** and **17**). The docking computations suggested that the loss of activity was mainly caused by the steric hindrance produced by the substitution in position 4. About the position 3, the substitution of the chlorine atom (**1**) with methoxy (**16**) group gave rise to inactive compounds. Also in this case, it seemed related with steric hindrance. On the contrary, the introduction of the methyl group (**12**) produced an active derivative with a slight improvement of the inhibitory concentration which might be related to a new contact between the methyl group and the Asn50 side chain (Fig. 4).

The analyses of derivative **12** binding mode reveal several crucial interactions. A salt bridge between the protonated secondary amine and the Glu12 side chain, a network of H-bonds involving the Asn50 side chain, and the ether oxygen atoms were observed. Also, hydrophobic interactions were observed between the 3′methoxyphenyl group and Trp35, the central phenyl ring with Tyr51, and the phenyl ring 1 with Phe7.

Worthily, the comparison of the binding modes showed that chlorine atom of derivative **1** was involved in halogen bond with Asn50 backbone, also the methyl group of **12** had hydrophobic contacts with Asn50 side chain. On the contrary, for the methoxy moiety (**16**) were not observed stabilizing interactions. (Fig. 4).

For the position 2 of phenyl ring 1, the introduction of a chlorine atom or a methyl cause the inactivity of compounds **7** and **14**, whereas the methoxy (**15**) moieties were well tolerated restoring the activity despite the decrease of K_d values compared to derivatives **12**. (Table 2 and Fig. 5).

Lastly, the effect of the introduction of another chlorine atom on the ring 3 was inspected keeping the 2-Cl atom on ring 1. This modification completely abolished the biological activity (**9**, **10** and **11**). In the same way, the shift of the methoxy group from position 4 to 2 produced inactive compound (**4**), whereas the movement from position 4 to 3 gave rise to less active derivative (**3**).

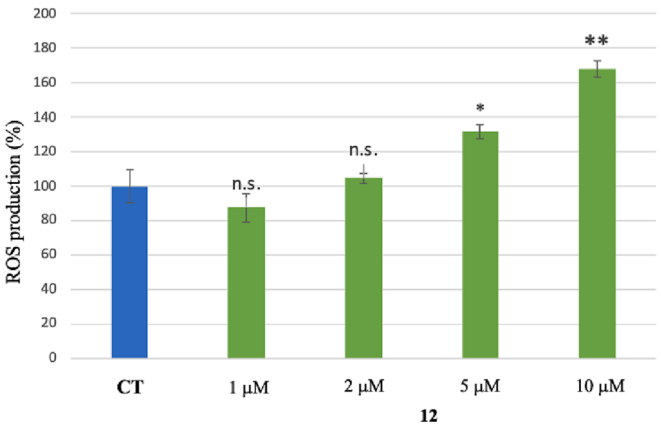

Fig. 7. ROS production for **12**. ROS production in H1299 cells upon treatment with different concentrations of **12**. The asterisks indicate statically significant differences between the effects induced by control (CT) and the derivative **12.**

The SAR analysis showed that the ethoxy group at ring 2 was pharmacophoric and the only acceptable change to the ring 3 was to place a methoxy group better in position 4′ than position 3′. Whereas the substitution in position 2′ was always forbidden. The substitutions for ring 1 were well accepted in position 3, far less in position 2 and totally intolerable in position 4 (Fig. 6).

2.4. ROS production

Cellular metabolism, growth, differentiation, and apoptosis are all affected by reactive oxygen species (ROS). [42] In addition to being a recognized cause of cell death, high levels of ROS are also implicated in several pathways, the mechanism of which is not yet completely understood. [32].

We used the fluorescent probe 2′,7′-dichlorodihydrofluorescein diacetate (DCFDA) to determine derivative **12** ROS-producing potential in H1299 cells. Various concentrations of **12** were tested and the ROS production (%) estimated after 48 h of treatment. The results indicate that ROS generation increases with increasing doses of drug (Fig. 7). Thus, a high level of ROS production was observed in studied cell after treatment with **12** at concentration higher than 5 μM for 48 h.

2.5. Drug-like properties and metabolic data

Compound **12** ADME profile was evaluated by computing the most representative chemical physical descriptors. (Table 2 SI). The compound is predicted to have a good absorption after oral administration with 0 violation of the rule of five. [33].

Derivative **12** phase I oxidative metabolic stability was experimentally measured (Table 3SI), with 7-ethoxycoumarin (7-EC) and propranolol as controls. The studied compound was highly metabolized after incubation with both mouse and human liver microsomes, showing a clearance closer to the propranolol than to 7-EC. Even though this result was far to be suitable, the following optimization steps will be focus to mask or to change the molecule sites more prone to metabolic transformation and to improve the anti-proliferative activity.

With this goal in mind, the atoms that might be more labile for Cyp 450 dependent metabolism were predicted. According to our calculations, the cytochromeP450 isoforms 3A4, 2D6, and 2C9 were more likely to metabolize carbon atoms connected to nitrogen and sp3 oxygen. (Fig. 6 SI and 7SI).

3. Conclusion

The crucial role of the Grb2/Gab2 complex in tumour development is well established [10] and it is also validated the effectiveness of Grb2 inhibition to arrests cancer proliferation. [17] Recently, derivative **1** was reported as a promising inhibitor of the Grb2 [29] and herein a first series of **1** analogues is described. The newly synthesized compounds were firstly assayed in equilibrium and kinetic binding experiments to confirm that the target was the cSH3 domain of Grb2. 5 out of the 18 tested compounds had K_D vales $\leq$ of 1and was able to antagonize the Grb2/Gab2 assembly. Then, the anti-proliferative activity was evaluated in H1299, SKOV3 and U87 cell lines. Derivative **12** showed a promising anticancer activity with inhibitory concentration in the range of one-digit μM concentration with a worthy value of 1.67 μM for H1299 cell. Also compound **12** produced a high level of ROS for H1299 cell at 5 and 10 μM concentrations for 48 h. By docking analyses, it was possible to rationalize an early structure activity relationship. Despite the promising anti-cancer activity compound **12** was rapidly metabolized after incubation with liver microsomes. In-silico prediction revealed the atoms that are more susceptible to metabolic reactions. Further efforts will be devoted to fix the metabolic hurdles and to improve the anti-proliferative activity of **12.**

In general, the reported derivatives represent the first series of Grb2 inhibitors targeting the cSH3 domain and pave the wave for the development of new compounds.

4. Material and methods

4.1. Molecular modelling

All molecular modelling studies were performed on a MacPro dual 2.66 GHz Xeon running Ubuntu 20 LTS. The Gab2 structures were downloaded from the PDB, pdb code 2W0Z and 2VWF. [34] Hydrogen atoms were added to the protein, using Maestro protein preparation wizard [35] Ligand structures were built with Maestro and minimized using the MMFF94x force field until a rmsd gradient of 0.05 kcal/(mol·Å) was reached. The docking simulations were performed using Glide using all default settings used. [36] The salt bridge between the carboxylic function of the Glu16 and the secondary amine moiety of the docked inhibitors was constrained during the docking computation. The images in the manuscript were created with PyMOL. [37].

4.2. Site of metabolism prediction

The sites of metabolism predictions were carried out with SMARTcyp [38] and the Schrodinger module in Maestro [39]. Both engines were consistent in suggesting chemical moieties or atoms more prone to metabolism reactions.

4.3. Chemistry

All reagents and solvents were handled according to the material safety data sheet of the supplier and were used as purchased without further purification. Organic solutions were dried over anhydrous sodium sulphate. Evaporation of solvents was carried out on a Büchi Rotavapor R-300 equipped with a Büchi V-850 vacuum controller, a Büchi V-300 vacuum pump and a recirculating chiller F-305. Column chromatography was performed on columns packed with silica gel from Macherey-Nagel (70–230 mesh). Silica gel thin layer chromatography (TLC) cards from Macherey-Nagel (silica gel precoated aluminum cards with fluorescent indicator visualizable at 254 nm) were used for TLC. Developed plates were visualized with a Spectroline ENF 260C/FE UV apparatus. Melting points (mp) were determined on a Stuart Scientific SMP1 apparatus and are uncorrected. Infrared (IR) spectra were recorded on a PerkinElmer Spectrum 100 FT-IR spectrophotometer equipped with a universal attenuated total reflectance accessory and IR data acquired and processed by PerkinElmer Spectrum 10.03.00.0069 software. Band position and absorption ranges are given in cm^{-1}. Proton nuclear magnetic resonance (^{1}H NMR) spectra were recorded with a Bruker Avance (400 MHz) spectrometer in the indicated solvent, and the corresponding fid files were processed by MestreLab Research SL MestreReNova 14.0.0–23239 software. Chemical shifts of ^{1}H and ^{13}C NMR are expressed in δ units (ppm) from tetramethylsilane.

4.3.1. Ethyl 4-((4-bromophenyl)sulfonamido)benzoate (1). Already reported. [29].

4.3.1.1. General procedure for the preparation of compound 2–19.

4.3.1.1.1. N-(4-(benzyloxy)-3-ethoxybenzyl)-2-phenylethan-1-amine (2).. A mixture of **20** (0.050 g; 0.195 mmol), 2-phenethylamine (0.024 g; 0.195 mmol) was dissolved in absolute ethanol (0.8 mL) with 3 Å MS (0.2 g). After 1.5 h was added sodium borohydride (0.011 g; 0.292 mmol). The solution was stirred for 1 h, then quenched with water and extracted with dichloromethane. The organic layer was washed with brine, dried on Na_2SO_4 and filtered. Evaporation of solvent gave a residue that was purified by silica gel column chromatography (DCM:EtOH, 9.5:0.5) to give 0.016 g of **2** (22%), mp 55–57 °C (from ethanol). ^{1}H NMR (DMSO-d_6): δ 1.33 (t, J = 6.9 Hz, 3H), 1.91 (br s, disappeared after treatment with D_2O, 1H), 2.73–2.74 (m, 4H), 3.67 (s, 2H), 4.00 (q, J = 6.9 Hz, 2H), 5.07 (s, 2H), 6.78 (dd, J = 1.9 and 8.1 Hz, 1H), 6.93–6.96 (m, 2H), 7.16–7.21 (m, 3H), 7.26–7.28 (m, 2H), 7.29–7.34 (m, 1H), 7.37–7.41 (m, 2H) and 7.43–7.45 ppm (m, 2H). IR: ν 1300 and 2922 cm^{-1}.

4.3.1.1.2. N-(4-((3-chlorobenzyl)oxy)-3-ethoxybenzyl)-2-(3-methoxyphenyl)ethan-1-amine (3).. Synthesized as **2** starting from **21** and 3-methoxyphenethyl amine. Yield 35%, oil. ^{1}H NMR (DMSO-d_6): δ 1.33 (t, J = 7.0 Hz, 3H), 2.25 (br s, disappeared after treatment with D_2O, 1H), 2.69–2.70 (m, 4H), 3.63 (s, 2H), 3.72 (s, 3H), 4.00 (q, J = 7.0 Hz, 2H), 5.08 (s, 2H), 6.73–6.78 (m, 4H), 6.91–6.93 (m, 1H), 6.94–6.95 (m, 1H), 7.17 (t, J = 7.8 Hz, 1H), 7.36–7.44 (m, 3H) and 7.51–7.52 ppm (m, 1H). IR: ν 1251 and 2924 cm^{-1}.

4.3.1.1.3. N-(4-((3-chlorobenzyl)oxy)-3-ethoxybenzyl)-2-(2-methoxyphenyl)ethan-1-amine (4).. Synthesized as **2** starting from **21** and 2-methoxyphenethyl amine. Yield 45%, oil. ^{1}H NMR (DMSO-d_6): δ 1.34 (t, J = 7.0 Hz, 3H), 2.30 (br s, disappeared after treatment with D_2O, 1H), 2.67–2.75 (m, 4H), 3.68 (s, 2H), 3.75 (s, 3H), 4.02 (q, J = 7.0 Hz, 2H), 5.10 (s, 2H), 6.79 (dd, J = 2.0 and 8.2 Hz, 1H), 6.85 (t, J = 7.4 Hz, 1H), 6.93 (d, J = 8.3 Hz, 2H), 6.97–6.98 (m, 1H), 7.12 (dd, J = 1.8 and 7.4 Hz, 1H), 7.18 (td, J = 1.8 and 7.7 Hz, 1H), 7.36–7.44 (m, 3H), and 7.51–7.52 ppm (m, 1H). IR: ν 1236 and 2956 cm^{-1}.

4.3.1.1.4. N-(4-((3-chlorobenzyl)oxy)-3-ethoxybenzyl)-2-phenylethan-1-amine (5).. Synthesized as **2** starting from **21** and phenethyl amine. Yield 48%, oil. ^{1}H NMR (DMSO-d_6): δ 1.33 (t, J = 6.9 Hz, 3H), 2.28 (br s, disappeared after treatment with D_2O, 1H), 2.67–2.74 (m, 4H), 3.62 (s, 2H), 3.99 (q, J = 6.9 Hz, 2H), 5.08 (s, 2H), 6.76 (dd, J = 1.9 and 8.2 Hz, 1H), 6.91–6.94 (m, 2H), 7.15–7.21 (m, 3H), 7.25–7.28 (m, 2H), 7.36–7.44 (m, 3H), 7.51–7.52 ppm (m, 1H). IR: ν 1269 and 2899 cm^{-1}.

4.3.1.1.5. N-(4-((4-chlorobenzyl)oxy)-3-ethoxybenzyl)-2-(4-methoxyphenyl)ethan-1-amine (6).. Synthesized as **2** starting from **22** and 4-methoxyphenethyl amine. Yield 51%, oil. ^{1}H NMR (DMSO-d_6): δ 1.32 (t, J = 6.9 Hz, 3H), 2.34 (br s, disappeared after treatment with D_2O, 1H), 2.65–2.66 (m, 4H), 3.62 (s, 2H), 3.71 (s, 3H), 3.99 (q, J = 6.9 Hz, 2H), 5.06 (s, 2H), 6.76 (dd, J = 1.9 and 8.1 Hz, 1H), 6.83 (d, J = 8.2 Hz, 2H), 6.90–6.93 (m, 2H), 7.10 (d, J = 8.2 Hz, 2H) and 7.45–7.46 ppm (m, 4H). IR: ν 1244 and 2930 cm^{-1}.

4.3.1.1.6. N-(4-((2-chlorobenzyl)oxy)-3-ethoxybenzyl)-2-(4-methoxyphenyl)ethan-1-amine (7).. Synthesized as **2** starting from **23** and 4-methoxyphenethyl amine. Yield 34%, oil. ^{1}H NMR (DMSO-d_6): δ 1.31 (t, J = 6.9 Hz, 3H), 1.98 (br s, disappeared after treatment with D_2O, 1H), 2.65–2.66 (m, 4H), 3.62 (s, 2H), 3.71 (s, 3H), 4.00 (q, J = 6.9 Hz,

2H), 5.12 (s, 2H), 6.78 (dd, $J = 1.9$ and 8.2 Hz, 1H), 6.83 (d, $J = 8.5$ Hz, 2H), 6.92–6.94 (m, 2H), 7.10 (d, $J = 8.5$ Hz, 2H), 7.36–7.41 (m, 2H), 7.49–7.51 (m, 1H) and 7.58–7.60 ppm (m, 1H). IR: ν 1244 and 2931 cm^{-1}.

*4.3.1.1.7. N-(4-(benzyloxy)-3-ethoxybenzyl)-2-(4-methoxyphenyl) ethan-1-amine (**8**)..* Synthesized as **2** starting from **20** and 4-methoxyphenethyl amine. Yield 44%, oil. ^{1}H NMR (DMSO-d_6): δ 1.32 (t, $J = 7.0$ Hz, 3H), 1.91 (br s, disappeared after treatment with D_2O, 1H), 2.67–2.68 (m, 4H), 3.64 (s, 2H), 3.71 (s, 3H), 3.99 (q, $J = 7.0$ Hz, 2H), 5.06 (s, 2H), 6.77 (dd, $J = 1.9$ and 8.2 Hz, 1H), 6.83 (d, $J = 8.6$ Hz, 2H), 6.92–6.94 (m, 2H), 7.11 (d, $J = 8.6$ Hz, 2H), 7.30–7.34 (m, 1H) and 7.37–7.45 ppm (m, 4H). IR: ν 1266 and 2940 cm^{-1}.

*4.3.1.1.8. N-(4-((3-chlorobenzyl)oxy)-3-ethoxybenzyl)-2-(2-chlorophenyl)ethan-1-amine (**9**)..* Synthesized as **2** starting from **21** and 2-chlorophenethyl amine. Yield 30%, oil. ^{1}H NMR (DMSO-d_6): δ 1.34 (t, $J = 6.9$ Hz, 3H), 1.92 (br s, disappeared after treatment with D_2O, 1H), 2.70 (t, $J = 7.4$ Hz, 2H), 2.85 (t, $J = 7.4$ Hz, 2H), 3.64 (s, 2H), 4.00 (q, $J = 6.9$ Hz, 2H), 5.09 (s, 2H), 6.78 (dd, $J = 1.9$ and 8.2 Hz, 1H), 6.92 (d, $J = 8.1$ Hz, 1H), 6.95 (d, $J = 1.9$ Hz, 1H), 7.20–7.28 (m, 2H), 7.33–7.35 (m, 1H), 7.36–7.42 (m, 4H) and 7.51–7.52 (m, 1H). IR: ν 1259 and 2928 cm^{-1}.

*4.3.1.1.9. N-(4-((3-chlorobenzyl)oxy)-3-ethoxybenzyl)-2-(3-chlorophenyl)ethan-1-amine (**10**)..* Synthesized as **2** starting from **21** and 3-chlorophenethyl amine. Yield 66%, mp 76–78 °C. ^{1}H NMR (DMSO-d_6): δ 1.34 (t, $J = 7.0$ Hz, 3H), 2.10 (br s, disappeared after treatment with D_2O, 1H), 2.85–2.94 (m, 4H), 3.85 (s, 2H), 4.04 (q, $J = 7.0$ Hz, 2H), 5.12 (s, 2H), 6.88 (dd, $J = 1.9$ and 8.2 Hz, 1H), 6.99 (d, $J = 8.2$ Hz, 1H), 7.09 (d, $J = 1.9$ Hz, 1H), 7.19–7.21 (m, 2H), 7.28–7.34 (m, 3H), 7.36–7.43 (m, 3H) and 7.51–7.52 (m, 1H). IR: ν 1268 and 2754 cm^{-1}.

*4.3.1.2. N-(4-((3-chlorobenzyl)oxy)-3-ethoxybenzyl)-2-(4-chlorophenyl) ethan-1-amine (**11**)..* Synthesized as **2** starting from **21** and 4-chlorophenethyl amine. Yield 58%, oil. ^{1}H NMR (DMSO-d_6): δ 1.33 (t, $J = 7.0$ Hz, 3H), 2.13 (br s, disappeared after treatment with D_2O, 1H), 2.64–2.73 (m, 4H), 3.61 (s, 2H), 3.98 (q, $J = 7.0$ Hz, 2H), 5.08 (s, 2H), 6.76 (dd, $J = 1.9$ and 8.2 Hz, 1H), 6.90–6.92 (m, 2H), 7.23 (d, $J = 8.2$ Hz, 2H), 7.31 (d, $J = 8.3$ Hz, 2H), 7.36–7.44 (m, 3H) and 7.51–7.52 (m, 1H). IR: ν 1260 and 2916 cm^{-1}.

*4.3.1.2.1. N-(3-ethoxy-4-((3-methylbenzyl)oxy)benzyl)-2-(4-methoxyphenyl)ethan-1-amine (**12**)..* Synthesized as **2** starting from **24** and 4-methoxyphenethyl amine. Yield 58%, oil. ^{1}H NMR (DMSO-d_6): δ 1.32 (t, $J = 6.9$ Hz, 3H), 2.02 (br s, disappeared after treatment with D_2O, 1H), 2.32 (s, 3H), 2.65–2.66 (m, 4H), 3.62 (s, 2H), 3.71 (s, 3H), 3.99 (q, $J = 6.9$ Hz, 2H), 5.01 (s, 2H), 6.76 (dd, $J = 1.9$ and 8.1 Hz, 1H), 6.83 (d, $J = 8.5$ Hz, 2H), 6.91–6.93 (m, 2H), 7.10–7.14 (m, 3H) and 7.21–7.29 ppm (m, 3H). IR: ν 1245 and 2917 cm^{-1}.

*4.3.1.2.2. N-(3-ethoxy-4-((4-methylbenzyl)oxy)benzyl)-2-(4-methoxyphenyl)ethan-1-amine (**13**)..* Synthesized as **2** starting from **25** and 4-methoxyphenethyl amine. Yield 58%, oil. ^{1}H NMR (DMSO-d_6): δ 1.31 (t, $J = 6.9$ Hz, 3H), 2.11 (br s, disappeared after treatment with D_2O, 1H), 2.30 (s, 3H), 2.64–2.65 (m, 4H), 3.61 (s, 2H), 3.71 (s, 3H), 3.99 (q, $J = 6.9$ Hz, 2H), 5.00 (s, 2H), 6.74 (dd, $J = 1.9$ and 8.2 Hz, 1H), 6.83 (d, $J = 8.4$ Hz, 2H), 6.89–6.91 (m, 2H), 7.10 (d, $J = 8.4$ Hz, 2H), 7.19 (d, $J = 7.7$ Hz, 2H) and 7.31 (d, $J = 7.7$ Hz, 2H). IR: ν 1244 and 2926 cm^{-1}.

*4.3.1.2.3. N-(3-ethoxy-4-((2-methylbenzyl)oxy)benzyl)-2-(4-methoxyphenyl)ethan-1-amine (**14**)..* Synthesized as **2** starting from **26** and 4-methoxyphenethyl amine. Yield 50%, oil. ^{1}H NMR (DMSO-d_6): δ 1.31 (t, $J = 6.9$ Hz, 3H), 2.19 (br s, disappeared after treatment with D_2O, 1H), 2.34 (s, 3H), 2.65–2.67 (m, 4H), 3.63 (s, 2H), 3.71 (s, 3H), 3.98 (q, $J = 6.9$ Hz, 2H), 5.03 (s, 2H), 6.78 (dd, $J = 1.9$ and 8.2 Hz, 1H), 6.83 (d, $J = 8.5$ Hz, 2H), 6.92 (d, $J = 1.9$ Hz, 1H), 6.97 (d, $J = 8.1$ Hz, 1H), 7.11 (d, $J = 8.5$ Hz, 2H), 7.17–7.26 (m, 3H) and 7.39–7.40 ppm (m, 1H). IR: ν 1245 and 2929 cm^{-1}.

*4.3.1.2.4. N-(3-ethoxy-4-((2-methoxybenzyl)oxy)benzyl)-2-(4-methoxyphenyl)ethan-1-amine (**15**)..* Synthesized as **2** starting from **27** and 4-methoxyphenethyl amine. Yield 48%, oil. ^{1}H NMR (DMSO-d_6): δ 1.31 (t, $J = 7.0$ Hz, 3H), 1.91 (br s, disappeared after treatment with D_2O, 1H), 2.65–2.66 (m, 4H), 3.62 (s, 2H), 3.71 (s, 3H), 3.82 (s, 3H), 3.99 (q, $J = 7.0$ Hz, 2H), 5.02 (s, 2H), 6.76 (dd, $J = 1.9$ and 8.2 Hz, 1H), 6.83 (d, $J = 8.4$ Hz, 2H), 6.89 (d, $J = 8.1$ Hz, 1H), 6.92 (d, $J = 1.9$ Hz, 1H), 6.94–6.98 (m, 1H), 7.03–7.05 (m, 1H), 7.11 (d, $J = 8.4$ Hz, 2H), 7.32 (td, $J = 1.8$ and 7.8 Hz, 1H) and 7.40 ppm (dd, $J = 1.8$ and 7.4 Hz, 1H). IR: ν 1242 and 2932 cm^{-1}.

*4.3.1.2.5. N-(3-ethoxy-4-((3-methoxybenzyl)oxy)benzyl)-2-(4-methoxyphenyl)ethan-1-amine (**16**)..* Synthesized as **2** starting from **28** and 4-methoxyphenethyl amine. Yield 31%, oil. ^{1}H NMR (DMSO-d_6): δ 1.33 (t, $J = 6.9$ Hz, 3H), 1.98 (br s, disappeared after treatment with D_2O, 1H), 2.64–2.66 (m, 4H), 3.62 (s, 2H), 3.71 (s, 3H), 3.75 (s, 3H), 3.99 (q, $J = 6.9$ Hz, 2H), 5.03 (s, 2H), 6.76 (dd, $J = 1.9$ and 8.2 Hz, 1H), 6.83 (d, $J = 8.2$ Hz, 2H), 6.86–6.89 (m, 1H), 6.90–6.92 (m, 2H), 6.98–7.01 (m, 2H), 7.10 (d, $J = 8.2$ Hz, 2H) and 7.29 ppm (t, $J = 7.8$ Hz, 1H). IR: ν 1246 and 2933 cm^{-1}.

*4.3.1.2.6. N-(3-ethoxy-4-((4-methoxybenzyl)oxy)benzyl)-2-(4-methoxyphenyl)ethan-1-amine (**17**)..* Synthesized as **2** starting from **29** and 4-methoxyphenethyl amine. Yield 32%, mp 65–67 °C. ^{1}H NMR (DMSO-d_6): δ 1.31 (t, $J = 7.0$ Hz, 3H), 2.13 (br s, disappeared after treatment with D_2O, 1H), 2.64–2.66 (m, 4H), 3.61 (s, 2H), 3.71 (s, 3H), 3.75 (s, 3H), 3.97 (q, $J = 7.0$ Hz, 2H), 4.96 (s, 2H), 6.75 (dd, $J = 2.0$ and 8.1 Hz, 1H), 6.83 (d, $J = 8.5$ Hz, 2H), 6.90–6.96 (m, 4H), 7.10 (d, $J = 8.5$ Hz, 2H) and 7.36 ppm (d, $J = 8.5$ Hz, 1H). IR: ν 1243 and 2929 cm^{-1}.

*4.3.1.2.7. N-(4-((3-chlorobenzyl)oxy)benzyl)-2-(4-methoxyphenyl) ethan-1-amine (**18**)..* Synthesized as **2** starting from **30** and 4-methoxyphenethyl amine. Yield 70%, mp 220–224 °C. ^{1}H NMR (DMSO-d_6): δ 1.40 (br s, disappeared after treatment with D_2O, 1H), 2.73–2.85 (m, 4H), 3.72 (s, 3H), 3.83 (s, 2H), 5.13 (s, 2H), 6.86 (d, $J = 8.4$ Hz, 2H), 7.00 (d, $J = 8.3$ Hz, 2H), 7.13 (d, $J = 8.3$ Hz, 2H), 7.32 (d, $J = 8.2$ Hz, 2H), 7.40–7.42 (m, 3H) and 7.51–7.52 ppm (m, 1H). IR: ν 1244 and 2902 cm^{-1}.

*4.3.1.2.8. 2-(4-chlorophenyl)-N-(3-ethoxy-4-((3-methoxybenzyl)oxy) benzyl)ethan-1-amine (**19**)..* Synthesized as **2** starting from **28** and 4-chlorophenethyl amine. Yield 29%, oil. ^{1}H NMR (DMSO-d_6): δ 1.33 (t, $J = 6.9$ Hz, 3H), 2.18 (br s, disappeared after treatment with D_2O, 1H), 2.65–2.73 (m, 4H), 3.61 (s, 2H), 3.75 (s, 3H), 3.98 (q, $J = 6.9$ Hz, 2H), 5.03 (s, 2H), 6.75 (dd, $J = 1.9$ and 8.2 Hz, 1H), 6.86–6.89 (m, 1H), 6.90–6.92 (m, 2H), 6.98–7.01 (m, 2H), 7.23 (d, $J = 8.2$ Hz, 2H) and 7.29–7.33 ppm (m, 3H). IR: ν 1262 and 2930 cm^{-1}.

General procedure for the preparation of compound **20**–**30** at supplementary information.

4.4. Equilibrium and kinetic binding experiments

Equilibrium binding experiments were performed on a Fluoromax-4 single photon counting spectrofluorometer (Jobin-Yvon, NJ, USA). Buffer used was Hepes 50 mM, DMSO 20% v/v, pH 7.0 and the temperature was set at 25 °C. In the experiments, a constant concentration of c-SH3 (1 μM) was mixed with increasing concentrations of dansylated $Gab2_{503\text{-}524}$ (from 1 μM to 20 μM), in the absence and presence of a constant concentration (5 μM) of inhibitor molecules (**2**–**19**). Samples were excited at 280 nm and the quenching of Trp fluorescence emission by the dansylated peptide was followed. Binding tests between the cSH3 domain and inhibitor molecules were performed by mixing a constant concentration of cSH3 (1 μM) versus increasing concentrations of inhibiting moleules, exciting the sample at 280 nm and collecting fluorescence signals. Buffer used was Hepes 50 mM, DMSO 20% v/v, pH 7.0. Kinetic binding experiments were performed on a SX-18 Stopped-Flow Apparatus (Applied Photophysics). A constant concentration of c-SH3 (1 μM) was rapidly mixed with increasing concentrations of dansylated Gab2503-524 (from 4 μM to 10 μM), in the absence and presence of a constant concentration (5 μM) of inhibitor molecules (Fig. 1).

Samples were excited at 280 nm and single exponential fluorescence decays were followed by using a 330 ± 30 nm bandpass filter. 3 to 5 independent traces were acquired and averaged for each experiment. Buffer used was Hepes 50 mM, DMSO 20% v/v, pH 7.0 and the temperature was 25 °C.

4.5. Cellular assays

Cell lines: H1299, U87, SKOV3 were purchased form ATCC (Manassas, VA, USA).

H1299 were grown in RPMI-1640 medium (R8758, Sigma-Aldrich), supplemented with 100 IU/mL penicillin–streptomycin (P4458; Sigma-Aldrich) and 10% foetal bovine serum (F7524; Sigma-Aldrich).

U87 were grown in DMEM high glucose medium (D6429, Sigma-Aldrich) supplemented with 100 IU/mL penicillin–streptomycin (P4458; Sigma-Aldrich), 10% foetal bovine serum (F7524; Sigma-Aldrich) and 1% non-essential amino acid (11140050, Thermo Fisher Scientific).

SKOV3 were grown in McCoy's 5A medium, supplemented with 100 IU/mL penicillin–streptomycin (P4458; Sigma-Aldrich) and 10% foetal bovine serum (F7524; Sigma-Aldrich).

4.5.1. Trypan blue exclusion assay (performed on all cell lines)

24 h after seeding, cells were treated with the different inhibitors (**1**, **3**, **5**, **8**, **12**, **15**) at different concentrations (1, 2, 5, 10 μM). 48 h after the treatment, the growth medium was collected, the cells were washed once with phosphate buffered saline (PBS). Adherent cells were removed by treatment with trypsin, which in turn was blocked using complete medium. All the collected cell fractions were centrifuged 5 min at 1000 rpm and the supernatant carefully discarded. The harvested cells were then washed with PBS, centrifuged 5 min at 1000 rpm and the supernatant discarded. Following the addition of a 0.4% (w/v) trypan blue stain solution (EBT-001, NanoEntek) cells were transferred to a cell counting slide (EVS-050, EveTM NanoEntek), visualized, and counted using EveTM Automatic Cell Counter, (NanoEntek). Cells stained with trypan blue dye were considered non-viable.

4.6. Reactive oxygen species (ROS) quantification (performed only on H1299)

Generation of ROS in H1299 cells was measured after 48 h exposure to **12** (1, 2, 5, 10 μM) by using the fluorescent probe 2,7-dichlorodihydrofluorescein diacetate (DCFDA, Sigma-Aldrich) in 96-well (black) plates. The relative fluorescence emission, after cell loading of DCFDA 10 μM, was followed at 520 nm (VICTOR™ Multilabel Counter, Perkin Elmer).

4.7. Statistical analysis of cell experiments

Statistical analysis was performed with the ANOVA test followed by the Bonferroni post hoc test, p value < 0.05 was considered significant.

4.8. In vitro oxidative metabolic stability

4.8.1. Intrinsic clearance in microsomes.

Mouse (Sigma Aldrich, CD-1 male, pooled) and human microsomes (Sigma Aldrich, human, pooled) at 0.5 mg/mL were preincubated with the test compound 15 dissolved in DMSO at 1 μM in phosphate buffer 50 mM, pH 7.4, and 3 mM $MgCl_2$ for 10 min at 37 °C. The reaction was then started by adding the cofactor mixture solution (NADP, glucose-6-phosphate, glucose-6-phosphate dehydrogenase in 2% $NaHCO_3$). Samples were taken at 0, 10, 30, 45 and 60 min and added to acetonitrile to stop the reaction. Samples were then centrifuged, and the supernatant was analyzed by LC-MS/MS to quantify the amount of compound. A control sample without cofactor was always added to check the chemical stability of the test compound. Two reference compounds of known metabolic stability, 7-EC and propranolol, were present in parallel testing. A fixed concentration of verapamil was added in every sample as an internal standard for LC-MS/MS analyses. The percentage of the area of the test compound remaining at the various incubation times was calculated with respect to the area of the compound at time 0 min.

The intrinsic clearance (Cli) was calculated by the following equation:

$$\text{Cli (μL/min/mg)} = \text{k/microsomal conc.} \times 1000$$

where k is the rate constant (min^{-1}); microsomal protein conc. = 0.5 mg protein/mL. The rate constant, k (min^{-1}) derived for the exponential decay equation (peak area/IS vs time), was used to calculate the rate of Cli. [40] In vitro stability is classified as low when the value is ≤ 2.5 (mouse) and ≤ 1.8 (human), medium when the value is 2.5 – 66 (mouse) and 1.8 – 48 (human), high for values > 66 (mouse) and > 48 (human) [32,41,43].

Table 3
Compound MRM transition and conditions.

Compound	Parent Ion	Product Ion	DP (V)	CE (eV)
7-EC	190.9	163.0	56	23
Propranolol	260.4	183.2	40	25
Verapamil	455.4	165.1	31	35
12	4	255.3	25	17

4.8.2. LC–MS/MS analytical method

Samples were analyzed under the following conditions: UPLC Waters coupled with an API 3200 triple-quadrupole (ABSciex); eluents, (phase A) 95% water, 5% acetonitrile + 0.1% HCOOH, (phase B) 5% water, 95% acetonitrile + 0.1% HCOOH; flow rate, 0.3 mL/min; column, Gemini-Nx 5 μm C18 110A (50 × 2.00 mm) at 35 °C; injection volume, 10 μL. LC–MS/MS analyses were carried out using an ESI(+) interface in multiple reaction monitoring (MRM) mode. Conditions and MRM transitions applied to the compounds are described in Table 3. Source conditions ESI positive: T 400 °C, Gas 1 45, Gas 2 40, CUR 50, IS 5500, CAD 5.

Declaration of Competing Interest

The authors declare the following financial interests/personal relationships which may be considered as potential competing interests: Romano Silvestri, Stefano Gianni reports financial support was provided by Italian Association for Cancer Research.

Data availability

Data will be made available on request.

Acknowledgements

Authors thank financial support: Associazione Italiana per la Ricerca su Cancro IG 2020, code no. 24703 to R.S.; Associazione Italiana per la Ricerca su Cancro IG 24551 to S.G.

Appendix A. Supplementary data

Supplementary data to this article can be found online at https://doi.org/10.1016/j.bioorg.2023.106607.

References

[1] M. Ijaz, F. Wang, M. Shahbaz, W. Jiang, A.H. Fathy, E.U. Nesa, The Role of Grb2 in Cancer and Peptides as Grb2 Antagonists, Protein Pept. Lett. 24 (12) (2018) 1084–1095.
[2] [Chardin P; Cussac D; Maignan S; Ducruix, A., The Grb2 adaptor, FEBS Lett. 369 (1) (1995) 47–51.

[3] T. Pawson, Dynamic control of signaling by modular adaptor proteins, Curr. Opin. Cell Biol. 19 (2) (2007) 112–116.
[4] Wagner MJ; Stacey MM; Liu BA; Pawson T. Molecular mechanisms of SH2- and PTB-domain-containing proteins in receptor tyrosine kinase signaling. Cold Spring Harb Perspect Biol. 2013, 5(12):a008987.
[5] T.J. Liao, H. Jang, R. Nussinov, D. Fushman, High-affinity Interactions of the nSH3/cSH3 Domains of Grb2 with the C-terminal Proline-rich Domain of SOS1, J. Am. Chem. Soc. 142 (7) (2020) 3401–3411.
[6] T. Xiao, L. Sun, M. Zhang, Z. Li, E.B. Haura, E. Schonbrunn, H. Ji, Synthesis and structural characterization of a monocarboxylic inhibitor for GRB2 SH2 domain, Bioorg. Med. Chem. Lett. 51 (2021), 128354.
[7] C.B. Ding, W.N. Yu, J.H. Feng, J.M. Luo, Structure and function of Gab2 and its role in cancer, Mol. Med. Rep. 12 (3) (2015) 4007–4014.
[8] A. Giubellino, T.R. Burke, Jr; Bottaro DP., Grb2 signaling in cell motility and cancer, Expert Opin. Ther. Targets 12 (8) (2008) 1021–1033.
[9] M. Sattler, M.G. Mohi, Y.B. Pride, L.R. Quinnan, N.A. Malouf, K. Podar, F. Gesbert, H. Iwasaki, S. Li, R.A. Van Etten, H. Gu, J.D. Griffin, B.G. Neel, Critical role for Gab2 in transformation by BCR/ABL, Cancer Cell 1 (5) (2002) 479–492.
[10] C. Ding, J. Luo, L. Li, S. Li, L. Yang, H. Pan, Q. Liu, H. Qin, C. Chen, J. Feng, Gab2 facilitates epithelial-to-mesenchymal transition via the MEK/ERK/MMP signaling in colorectal cancer, J. Exp. Clin. Cancer Res. 35 (5) (2016) 2–10.
[11] M. Bentires-Alj, S.G. Gil, R. Chan, Z.C. Wang, Y. Wang, N. Imanaka, L.N. Harris, A. Richardson, B.G. Neel, H. Gu, A role for the scaffolding adapter GAB2 in breast cancer, Nat. Med. 12 (2006) 114–121.
[12] S. Hak Lee, E. Goo Jeong, S. Woo Nam, J. Young Lee, N. Jin Yoo, S. Hyung Lee, Increased expression of Gab2, a scaffolding adaptor of the tyrosine kinase signalling, in gastric carcinomas, Pathology 39 (3) (2007) 326–329.
[13] X.L. Xu, X. Wang, Z.L. Chen, M. Jin, W. Yang, G.F. Zhao, J.W. Li, Overexpression of Grb2-associated binder 2 in human lung cancer, Int. J. Biol. Sci. 7 (2011) 496–504.
[14] S. Gu, W.W. Chan, G. Mohi, J. Rosenbaum, A. Sayad, Z. Lu, C. Virtanen, S. Li, B. G. Neel, R.A. Van Etten, Distinct GAB2 signaling pathways are essential for myeloid and lymphoid transformation and leukemogenesis by BCR-ABL1, Blood 127 (2016) 1803–1813.
[15] A. Zatkova, C. Schoch, F. Speleman, B. Poppe, C. Mannhalter, C. Fonatsch, K. Wimmer, GAB2 is a novel target of 11q amplification in AML/MDS, Genes Chromosom. Cancer 45 (9) (2006) 798–807.
[16] F.U. Wöhrle, R.J. Daly, T. Brummer, Function, regulation and pathological roles of the Gab/DOS docking proteins, Cell Commun. Signal. CCS 7 (2009) 22.
[17] C. Duckworth, L. Zhang, S.L. Carroll, S.P. Ethier, H.W. Cheung, Overexpression of GAB2 in ovarian cancer cells promotes tumor growth and angiogenesis by upregulating chemokine expression, Oncogene 35 (31) (2016) 4036–4047.
[18] Y. Ke, D. Wu, F. Princen, T. Nguyen, Y. Pang, J. Lesperance, W.J. Muller, R. G. Oshima, G.S. Feng, Role of Gab2 in mammary tumorigenesis and metastasis, Oncogene 26 (34) (2007) 4951–4960.
[19] G.Z. Yu, Y. Chen, J.J. Wang, Overexpression of Grb2/HER2 signaling in Chinese gastric cancer: their relationship with clinicopathological parameters and prognostic significance, J. Cancer Res. Clin. Oncol. 135 (10) (2009) 1331–1339.
[20] A.M. Pendergast, L.A. Quilliam, L.D. Cripe, C.H. Bassing, Z. Dai, N. Li, A. Batzer, K. M. Rabun, C.J. Der, J. Schlessinger, et al., BCR-ABL-induced oncogenesis is mediated by direct interaction with the SH2 domain of the GRB-2 adaptor protein, Cell 75 (1) (1993) 175–185.
[21] Y. Zhang, Z. Li, M. Yang, D. Wang, L. Yu, C. Guo, X. Guo, N. Lin, Identification of GRB2 and GAB1 coexpression as an unfavorable prognostic factor for hepatocellular carcinoma by a combination of expression profile and network analysis, PLoS One 8 (12) (2013) e85170.
[22] T. Watanabe, N. Shinohara, K. Moriya, A. Sazawa, Y. Kobayashi, Y. Ogiso, M. Takiguchi, J. Yasuda, T. Koyanagi, N. Kuzumaki, A. Hashimoto, Significance of the Grb2 and son of sevenless (Sos) proteins in human bladder cancer cell lines, IUBMB Life 49 (4) (2000) 317–320.
[23] H. Fretz, P. Furet, C. Garcia-Echeverria, J. Schoepfer, J. Rahuel, Structure-based design of compounds inhibiting Grb2-SH2 mediated protein-protein interactions in signal transduction pathways, Curr. Pharm. Des. 6 (2000) 1777–1796.
[24] T.K. Sawyer, R.S. Bohacek, D.C. Dalgarno, C.J. Eyermann, N. Kawahata, C. A. Metcalf 3rd, W.C. Shakespeare, R. Sundaramoorthi, Y. Wang, M.G. Yang, SRC homology-2 inhibitors: peptidomimetic and nonpeptide, Mini Rev. Med. Chem. 2 (5) (2002) 475–488.
[25] T.R. Burke, Development of Grb2 SH2 Domain Signaling Antagonists: A Potential New Class of Antiproliferative Agents, Int. J. Pept. Res. Ther. 12 (1) (2006) 33–48.
[26] D. Kraskouskaya, E. Duodu, C.C. Arpin, P.T. Gunning, Progress towards the development of SH2 domain inhibitors, Chem. Soc. Rev. 42 (8) (2013) 3337–3370.
[27] P. Morlacchi, F.M. Robertson, J. Klostergaard, J.S. McMurray, Targeting SH2 domains in breast cancer, Future Med. Chem. 6 (17) (2014) 1909–1926.
[28] P.C. Simister, J. Luccarelli, S. Thompson, D.H. Appella, S.M. Feller, A.D. Hamilton, Novel inhibitors of a Grb2 SH3C domain interaction identified by a virtual screen, Bioorg. Med. Chem. 21 (14) (2013) 4027–4033.
[29] F. Malagrinò, A. Coluccia, M. Bufano, G.L. Regina, M. Puxeddu, A. Toto, L. Visconti, A. Paone, M.C. Magnifico, F. Troilo, F. Cutruzzolà, R. Silvestri, S. Gianni, Targeting the Interaction between the SH3 Domain of Grb2 and Gab2, Cells 9 (2020) 2435.
[30] F. Malatesta, The study of bimolecular reactions under non-pseudo-first order conditions, Biophys. Chem. 116 (3) (2005) 251–256.
[31] E. Antonini, M. Brunorl, Hemoglobin and myoglobin in their reactionswith ligands, North-Holland, Amsterdam. The Netherlands, 1971.
[32] B. Perillo, M. Di Donato, A. Pezone, E. Di Zazzo, P. Giovannelli, G. Galasso, G. Castoria, A. Migliaccio, ROS in cancer therapy: the bright side of the moon, Exp. Mol. Med. 52 (2) (2020) 192–203.
[33] C.A. Lipinski, F. Lombardo, C.A. Dominy, P.J. Feeney, Experimental and computational approaches to estimate solubility and permeability in drug discovery and development settings, Adv. Drug Deliv. Rev. 46 (2001) 3–26.
[34] M. Harkiolaki, T. Tsirka, M. Lewitzky, P.C. Simister, D. Joshi, L.E. Bird, E.Y. Jones, N. O'Reilly, S.M. Feller, Distinct binding modes of two epitopes in Gab2 that interact with the SH3C domain of Grb2, Structure 17 (6) (2009) 809–822.
[35] G.M. Sastry, M. Adzhigirey, T. Day, R. Annabhimoju, W. Sherman, Protein and ligand preparation: parameters, protocols, and influence on virtual screening enrichments, J. Comput. Aided Mol. Des. 27 (3) (2013) 221–234.
[36] R.A. Friesner, R.B. Murphy, M.P. Repasky, L.L. Frye, J.R. Greenwood, T.A. Halgren, P.C. Sanschagrin, D.T. Mainz, Extra precision glide: docking and scoring incorporating a model of hydrophobic enclosure for protein-ligand complexes, J. Med. Chem. 49 (21) (2006) 6177–6196.
[37] [PyMOL version1.2r1. DeLanoScientificLLC: SanCarlos, CA.
[38] P. Rydberg, D.E. Gloriam, J. Zaretzki, C. Breneman, L. Olsen, SMARTCyp: A 2D Method for Prediction of Cytochrome P450-Mediated Drug Metabolism, ACS Med. Chem. Lett. 1 (3) (2010) 96–100.
[39] Maestro, Schrödinger, LLC, New York, NY, 2021.
[40] S.E. Clarke, P. Jeffrey, Utility of metabolic stability screening: comparison of in vitro and in vivo clearance, Xenobiotica 31 (8–9) (2001) 591–598.
[41] J. Brian Houston, Utility of in vitro drug metabolism data in predicting in vivo metabolic clearance, Biochem. Pharmacol. 47 (9) (1994) 1469–1479.
[42] R.J. Riley, D.F. McGinnity, R.P. Austin, A unified model for predicting human hepatic, metabolic clearance from in vitro intrinsic clearance data in hepatocytes and microsomes, Drug Metab. Dispos. 33 (2005) 1304–1311.
[43] B. Davies, T. Morris, Physiological parameters in laboratory animals and humans, Review Pharm. Res. 10 (1993) 1093–1095.